0013-4651/2011/158(8)/D463/6/$28.00 © The Electrochemical Society

Electroless Deposition of Ru Films Via an Oxidative-Reductive Mechanism

Jing-Yu Chen,* Yu-Chi Hsieh,* Li-Yeh Wang, and Pu-Wei Wu,z**

Department of Materials Science and Engineering, National Chiao Tung University Hsin-chu 300, Taiwan

An electroless Ru plating bath is prepared by mixing Ru precursor ($K_2RuCl_5{\cdot}xH_2O$), oxidizer (NaClO), stabilizer (NaOH), and reducing agent ($NaNO_2$) simultaneously in deionized water at a molar ratio of 1:1:20:10. Instead of conventional direct reduction route, the $RuCl_5^{2-}$ experiences an oxidative-reductive sequence to form metallic Ru on an activated Si substrate. Spectra from ultraviolet-visible and X-ray absorption spectroscopy indicate that the $RuCl_5^{2-}$ is oxidized to form RuO_4 initially, followed by a slight reduction becoming RuO_4^{2-}. The RuO_4^{2-} solution is relatively stable and is able to undergo further reduction to render metallic Ru via heterogeneous nucleation and growth. Images from scanning electron microscope demonstrate a solid film of 100 nm with scattered protrusions and cavities after 120 min plating time. Analysis from atomic force microscope determines its surface roughness of 7.8 nm. From X-ray diffraction patterns, the as-deposited film reveals an amorphous structure but turns crystalline after Ar annealing at 400°C for 2 h. Curve-fitting of Ru $3p_{3/2}$ signal from X-ray photoelectron spectroscopy suggests a film composition of 92.49 atom % Ru and 7.51 atom % RuO_2. The electroless Ru plating bath exhibits impressive life time (137 h) and negligible homogeneous precipitation without involving surfactants and unnecessary chemical additives.
© 2011 The Electrochemical Society. [DOI: 10.1149/1.3592996] All rights reserved.

Manuscript submitted March 17, 2011; revised manuscript received April 26, 2011. Published May 26, 2011. This was Paper 1977 presented at the Las Vegas, Nevada, Meeting of the Society, October 10–15, 2010.

Ruthenium (Ru) is a member of platinum group metals that is often employed in applications such as electrocatalysis for fuel cells, pseudocapacitors for energy storage, and barrier/seed layer for semiconductor devices.[1–6] So far, a variety of fabrication schemes has been explored to prepare the Ru and its oxides in thin solid films. For example, vacuum-based techniques including atomic layer deposition (ALD), physical vapor deposition (PVD), and chemical vapor deposition (CVD), as well as solution-based approaches like electroplating and electroless deposition have been demonstrated with impressive results.[4,5,7–16] In general, the vacuum-based techniques involve complicated equipment, costly precursors, slow processing time, and unnecessary material waste. In contrast, the electrochemical alternative provides attractive attributes in simple setups, facile processing, and adjustable growth rate. In electroplating, an external driving force of current or voltage is imposed to reduce relevant precursors in an electrolyte to the metallic form.[10] Hence, to obtain desirable deposit, the substrate requires sufficient electrical conductivity and planar contour for uniform distribution of electrical field. In contrast, the electroless deposition is performed via a chemical reducing agent that enables more freedoms in substrate selections and morphologies.[11,12,16,17] To date, electroless depositions of Ni, Cu, Ag, Au, Pd, and Pt have been widely studied and many of their formulations can be found in literature reports.[18–24] However, precious metals like Ru, Rh, Os, and Ir have received much less attention and their electroless baths warrant further investigations.[11–13,16,25]

So far, a few studies document the electroless deposition of Ru in which $RuCl_3$ was employed as the Ru precursor, and reducing agents such as N_2H_4, $NaBH_4$, and $NaH_2PO_2{\cdot}H_2O$ were utilized.[11–13,16] These work report direct morphology observations and material characterizations for the Ru deposits but fail to provide details on the reaction steps involved. It is because in electrolyte, the Ru precursor is known to exist in different oxidized forms, and a disporportionation reaction among them might render random precipitations via homogeneous nucleation and growth. This undesirable process is accelerated if the reducing agent reveals excess reducing power, a character shared by N_2H_4 and $NaBH_4$. Despite the $NaH_2PO_2{\cdot}H_2O$ exhibits a moderate reducing power, its decomposition always leads to residual phosphorus in the deposit.[19,26] The incorporation of impurities in the deposit during electroless plating is not uncommon especially chemicals such as complexing agents and surfactants are often added to prolong the bath life time and adjust its surface wettability.[13,16]

Recently, RuO_4 has been used as the precursor in CVD and ALD to produce Ru and RuO_2 films because its reaction products are simpler than alternative metalorganics.[7,9,27] The RuO_4 is a volatile compound at room temperature but dissolves easily in water.[28] Therefore, it is of particular interest to explore the RuO_4 for electroless deposition because it is a powerful oxidizer (strong tendency to be reduced).[29] Hence, a relatively weak reducing agent can be selected which allows less interference from the homogeneous nucleation and growth. Conventional electroless depositions proceed via a direct reduction route in which the dissolved precursors undergo a straightforward reductive deposition on activated substrates. Unfortunately, the RuO_4 is rather reactive in solution that always requires stabilizing additives. Therefore, an in-situ oxidation step is necessary to convert typical Ru precursors like $RuCl_5^{2-}$ or $RuCl_3$ to RuO_4, followed by a reductive process for Ru metal deposition. As a result, we anticipate to develop an operational electroless Ru bath for improved chemical stability, reduced material waste, and less contamination.

In this work, we demonstrate an oxidative-reductive reaction sequence to deposit Ru electrolessly on activated Si substrates. Analysis of the plating bath and characterizations on the deposit are carried out so possible reaction steps are proposed and discussed.

Experimental

The electroless Ru deposition proceeded via an oxidative-reductive route in which the Ru precursor underwent an oxidation reaction first becoming intermediates with higher oxidized states followed by reacting with a reducing agent to convert to the metallic form. The electroless plating bath included 0.0186 g $K_2RuCl_5{\cdot}xH_2O$ (Alfa Aesar), 1.8558 g NaClO (SHOWA), 0.04 g NaOH (Mallinchrodt), and 0.035 g $NaNO_2$ (SHOWA) in 30 ml deionized water. They were used as the Ru precursor, oxidizer, stabilizer, and reducing agent, and their molarities were 1.64×10^{-3}, 1.66×10^{-3}, 3.33×10^{-2}, and 1.7×10^{-2} M, respectively. In preparing the plating bath, the $NaNO_2$ and NaOH were dissolved separately in deionized water followed by mixing with the NaClO solution. At this stage, both reducing agent and oxidizer were present. Subsequently, the mixture was added to an aqueous solution of $K_2RuCl_5{\cdot}xH_2O$ forming a homogeneous solution ready for Ru deposition. Since the NaClO was prone to decomposition, the NaOH was added to stabilize the bath. As a result, the *p*H value for the plating bath was between 11 and 12. For comparison purpose, we also prepared a reference bath by dissolving the NaOH in deionized water followed by

* Electrochemical Society Student Member.
** Electrochemical Society Active Member.
z E-mail: ppwu@mail.nctu.edu.tw

Downloaded on 2014-04-24 to IP 140.113.38.11 address. Redistribution subject to ECS terms of use (see ecsdl.org/site/terms_use) unless CC License in place (see abstract).

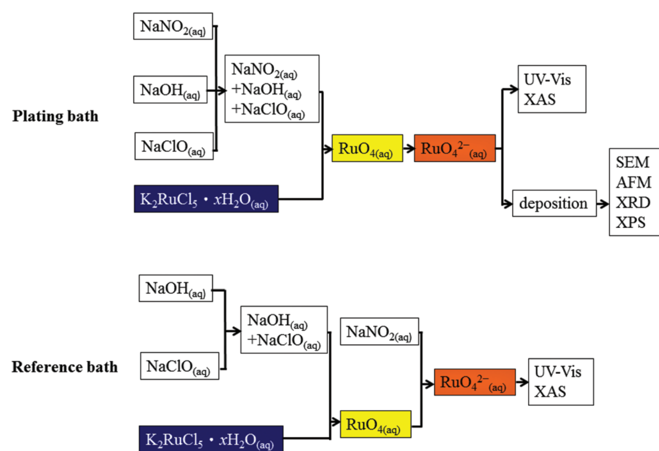

Figure 1. (Color online) A experimental flow chart for the processing steps and characterization tools involved in the electroless Ru deposition.

mixing with the NaClO solution. Subsequently, the mixture was added to an aqueous solution of $K_2RuCl_5 \cdot xH_2O$ allowing complete oxidization of the Ru precursor. Afterward, the $NaNO_2$ solution was added to the oxidized precursor to render a homogeneous solution. All the preparation steps were conducted at 25°C using as-received chemicals without further purification. A flow chart for the processing steps involved is depicted in Fig. 1.

Electroless Ru deposition was performed at 40°C on a Si substrate with surface coating of SiO_2 (500 nm), TaN (20 nm), and Cu (100 nm). This $Cu/TaN/SiO_2/Si$ arrangement is often adopted for semiconductor processing purpose. The Si substrate was broken into small pieces in 2×2 cm^2 and cleaned thoroughly by acetone and water. Prior to the electroless Ru deposition, the Si substrate was subjected to an activation step at 40°C by immersing in a solution containing 0.1 wt % $PdCl_2$ (Aldrich) and 1 wt % HCl (SHOWA) for 10 s. During electroless Ru deposition, the plating bath was raised to 40°C to allow a faster deposition rate. To improve the crystallinity of the as-deposited Ru film, an Ar annealing treatment was imposed at 400°C for 2 h.

Since the Ru precursors in different oxidized forms revealed distinct colors, measurements of the UV-Vis spectra during plating bath preparation enabled the determination of their identities and relative quantities. An UV-Vis spectrometer (JASCO V-670) was used to record the absorption curves at 25 and 40°C, respectively. X-ray absorption spectroscopy (XAS) of Ru K-edge was also adopted to confirm the chemical nature of Ru precursors prior to the electroless deposition. The XAS spectra were obtained from BL17C1 beam line at the National Synchrotron Radiation Research Center at Hsinchu, Taiwan. The photon energy was calibrated by the K-edge of metallic Ru sheet and the XAS data were recorded in a fluorescence mode at 25°C in air. The resulting spectra were processed by a program (Athena, version 0.8.056) in which the Ru K-edge absorption steps were normalized to unity with removal of background signals. Detailed XAS measurement procedures and data process protocols can be found elsewhere.[30]

A field-emission scanning electron microscope (FE-SEM; JOEL JSM-6500) was used to observe the morphology for the as-deposited Ru film and its surface roughness was determined by an atomic force microscope (AFM; Vecco Dimension 5000 Scanning Probe Microscopy). A high-resolution X-ray diffractometer (XRD; Bruker D8 Discover) was employed to identify the crystallinity and phase for the as-deposited and Ar-annealed Ru films. An X-ray photoelectron spectrometer (XPS; Thermo Microlab 350) was adopted to analyze the amount of Ru and RuO_2 in the as-deposited film. Prior to the XPS measurements, additional Pt was sputtered on the sample and used as the calibration at 71.3 eV ($4f_{7/2}$). During the XPS measurements, the sample was bombarded by Ar ions for 30 s to clean its surface. The XPS background was added with the Shirley method by a program (Thermo Avantage, version 3.20). All curve fittings were carried out at fixed binding energy for Ru and RuO_2 with identical full width at half maximum (FWHM).

Results and Discussion

The Ru precursors are known to reveal distinct colors contingent on their oxidation states and complexing ligands. This characteristic is rather useful especially when the aqueous solutions of NaClO, NaOH, and $NaNO_2$ are transparent. The $K_2RuCl_5 \cdot xH_2O$ solution appeared in dark blue and once it was added to the mixture of NaClO, NaOH, and $NaNO_2$, the solution became yellow shortly and its color turned orange for a few minutes. A similar yellow-to-orange transition was observed for the reference bath. As the $K_2RuCl_5 \cdot xH_2O$ solution was mixed with NaClO and NaOH, its color was converted and stabilized in yellow. Upon the addition of $NaNO_2$, the yellow solution changed to orange gradually. Since the NaClO and $NaNO_2$ functioned as the oxidizer and reducing agent respectively, we rationalized that the yellow color was indicative of Ru precursor in a higher oxidized state while the orange one inferred the Ru precursor in a slightly lower oxidized state. Figure 2 provides the UV-Vis absorption spectra for the plating bath during bath preparation at 25°C. The absorption peaks at 313 and 382 nm were identified and their intensities were decreasing gradually with time. According to literature, both RuO_4 and RuO_4^- display characteristic absorption peaks at these wavelengths but their relative intensities differ greatly.[31] Therefore, we realized that RuO_4 and RuO_4^- were present simultaneously at this stage and the predominant constituent was RuO_4. After 7 min, there appeared additional absorption peaks at 373 and 468 nm, and their intensities were increasing steadily with time. These absorption peaks were consistent with typical responses associated with RuO_4^{2-}.[31] Hence, the UV-Vis spectra suggested that the $RuCl_5^{2-}$ in the plating bath was oxidized first to RuO_4 (see Eq. 1 below) followed by a moderate reduction to RuO_4^{2-} at a later stage (see Eq. 2 below). It is noted that according to literature, the color for RuO_4, RuO_4^-, and RuO_4^{2-} aqueous solutions are yellow, green, and orange.[32] The absence of green color in our plating bath inferred that the presence of RuO_4^- was transient and the stabilized forms were RuO_4 and RuO_4^{2-}, respectively.

In our experiences, once the $RuCl_5^{2-}$ was transformed to the RuO_4^{2-}, it was able to react slowly with the $NaNO_2$ nearby for further reduction (see Eq. 5 below). To explore the operation life time for the plating bath, we carried out additional UV-Vis measurements at 40°C and the resulting absorption curves are exhibited in Fig. 3. Consistent with what we observed in Fig. 2, the absorption peaks at

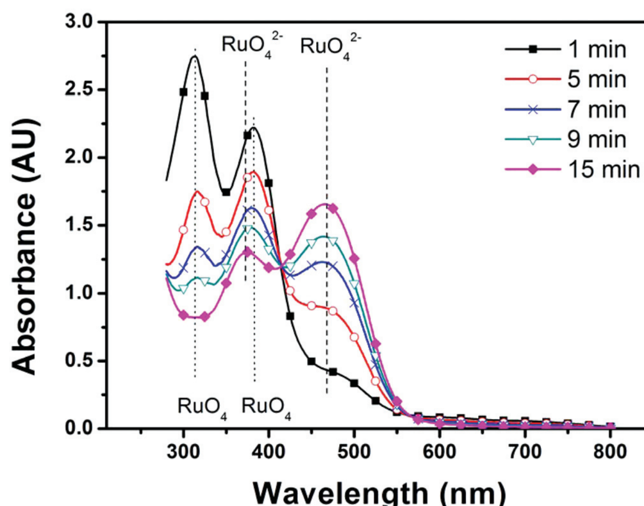

Figure 2. (Color online) UV-Visible spectra for the electroless Ru bath during preparation process at 25°C.

Downloaded on 2014-04-24 to IP 140.113.38.11 address. Redistribution subject to ECS terms of use (see ecsdl.org/site/terms_use) unless CC License in place (see abstract).

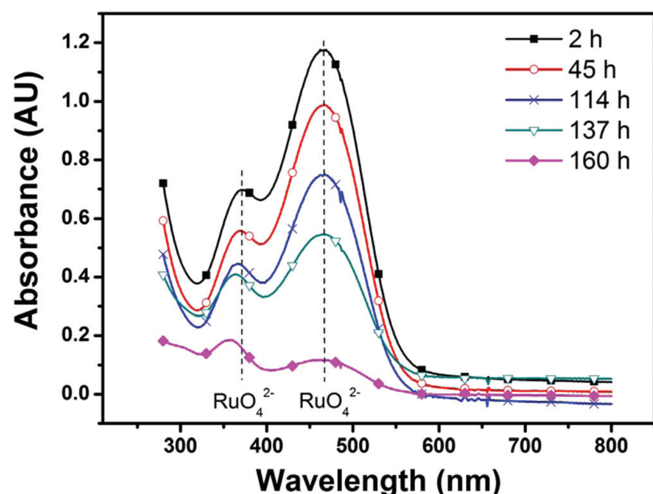

Figure 3. (Color online) UV-Visible spectra for the electroless Ru bath during deposition process at 40°C.

373 and 468 nm were identified. However, their intensity ratio remained unchanged whereas their absolute absorbance was reduced significantly as time progressed. This indicated that the concentration of the RuO_4^{2-} in the plating bath was decreasing steadily. In conjunction with the loss of RuO_4^{2-}, we noticed the formation of dark precipitates scattered on the side walls and at the bottom of the container (see Eqs. 3–5 below). Nevertheless, we did not observe any suspended precipitates in the plating bath. This suggested that the undesirable homogeneous nucleation and growth of Ru from the RuO_4^{2-} was not occurring at a noticeable rate, and the prevailing process was the heterogeneous nucleation and growth on the foreign surface. This behavior is rather encouraging as we expect the heterogeneous nucleation and growth becomes accelerated once the activated Si substrate is encountered with the RuO_4^{2-}. From Fig. 3, the life time for the plating bath is reasonably estimated at 137 h.

To validate sequential oxidative and reductive steps were taking place for the $RuCl_5^{2-}$, we conducted the XAS measurements on the plating and reference baths separately to record the Ru K-edge absorption energy. In general, the XAS spectra consist of X-ray absorption near edge structure (XANES) and extended X-ray absorption fine structure (EXAFS). In XANES, the oxidation state for the absorbing ions can be determined accurately by comparing their absorption energy with known samples. It is because the oxidized species are recognized to render a shift of the absorption peak to higher photon energy and the extent for the energy shift is proportional to the oxidized state of the absorbing ions. For EXAFS, relevant information including bond distance, coordination number of nearest neighboring elements, and atomic species around the absorbing ions can be obtained. Figure 4 presents the XANES spectra of Ru K-edge for Ru metal, aqueous solution of $K_2RuCl_5{\cdot}xH_2O$, aqueous solution of RuO_4 prepared by mixing $K_2RuCl_5{\cdot}xH_2O$, NaOH, and NaClO, as well as the electroless Ru and reference baths, respectively. As shown, the RuO_4 solution demonstrated the largest absorption energy while the Ru metal exhibited the least one. Accordingly, their respective curve indicated the oxidation state of 8 and 0. Interestingly, both the electroless Ru and reference baths revealed closely similar profiles indicating their oxidation states were identical. In addition, their absorption energy was notably larger than that of $K_2RuCl_5{\cdot}xH_2O$ which suggested that the oxidation state of Ru precursor at this stage was much larger than 3 but slightly smaller than 8. These results substantiated our premise that the Ru precursor existed as RuO_4^{2-} prior to the reductive deposition. Moreover, the Ru precursor was present in the same RuO_4^{2-} entity regardless the oxidizer and reducing agent were added simultaneously or sequentially. It is noted that using an in-situ XAS setup to analyze possible variation in the oxidation state for the Ru precursor during plating bath preparation was not applicable because each XAS measurement in our work required 120 min for data collection.

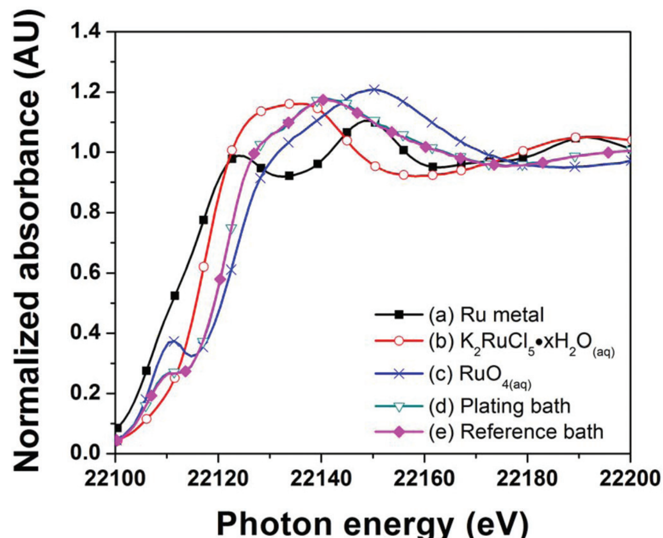

Figure 4. (Color online) Ru K-edge XANES spectra of metallic Ru and aqueous solutions of $K_2RuCl_5{\cdot}xH_2O$, RuO_4, and RuO_4^{2-} from plating bath and reference bath.

As the $RuCl_5^{2-}$ was converted to RuO_4^{2-}, the heterogeneous nucleation and growth was able to take place once the activated Si substrate was immersed in the plating bath. Figures 5a–5b demonstrate the planar and cross-sectional SEM images for the as-deposited Ru film after 120 min plating time. As shown in Fig. 5a, the surface morphology for the as-deposited Ru film was relatively uniform with scattered protrusions and cavities. The root-mean-square roughness from the AFM measurement was 7.8 nm. Figure 5b exhibits the cross-sectional view in which individual layers of TaN, Cu, and Ru were clearly visible. Apparently, the as-deposited Ru film displayed impressive integrity and the surface cavities in Fig. 5a were not penetrating to the underlying Cu layer. From the SEM image, the thickness for the as-deposited Ru film was approximately 100 nm. Shown in Figs. 5c and 5d are the SEM images in planar and cross-sectional views for the Ru film after Ar annealing. It can be seen from these images that the integrity of the Ru film was reasonably maintained and the surface morphology became

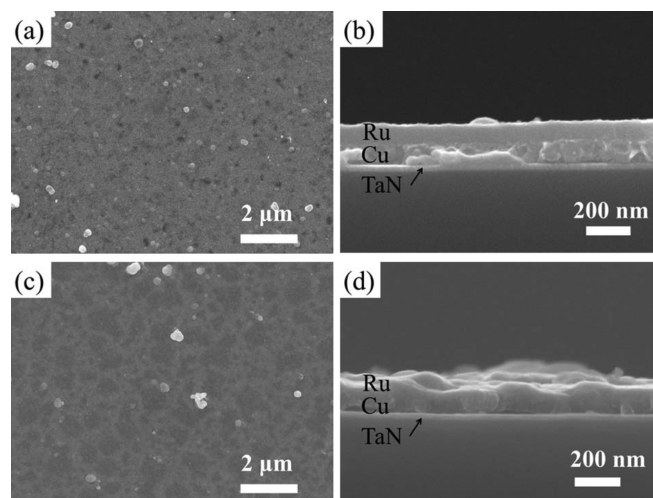

Figure 5. SEM images for the as-deposited film in (a) planar and (b) cross-sectional views, as well as Ar-annealed film in (c) planar and (d) cross-sectional view.

Downloaded on 2014-04-24 to IP 140.113.38.11 address. Redistribution subject to ECS terms of use (see ecsdl.org/site/terms_use) unless CC License in place (see abstract).

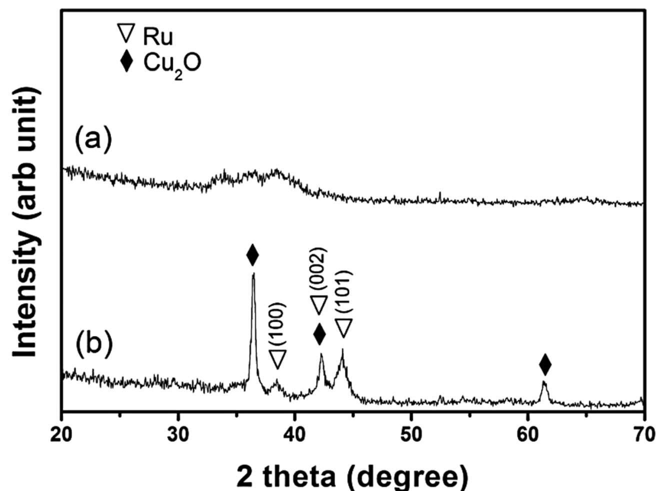

Figure 6. XRD patterns for the (a) as-deposited film and (b) film after Ar annealing at 400°C for 2 h.

rather rough suggesting crystallinity alteration during the annealing process.

Figure 6 provides the XRD patterns for the as-deposited and Ar annealed Ru films, respectively. As shown in Fig. 6a, the as-deposited Ru film exhibited an amorphous characteristic without discernible diffraction peaks. We understood that the noises between 33 and 37° were attributed to the Si substrate because a Si wafer before electroless plating demonstrated a similar pattern. This amorphous nature was not unexpected as earlier reports of electroless-derived Ru often revealed an amorphous structure.[13,14] Figure 6b presents the XRD pattern for the Ru film after Ar annealing. Notably, there appeared clear diffraction peaks associated with crystalline phases of Ru and Cu_2O. For example, diffraction signals of Ru at 38.5° (110), 42.3° (002), and 44.1° (101) were visible and their relative intensities agreed reasonably with those from JCPDS 060663. The grain size calculated with Scheerer's formula at 44.1° is 20.04 nm. In addition, diffraction peaks from the Cu_2O at 36.5° (111), 42.3° (200), and 61.4° (220) were observed. It is understood that the Cu diffuses rapidly at elevated temperature and it is possible that the Cu diffused to the external surface during Ar annealing. However, we believed that the formation of Cu_2O in our case was not caused by the out-diffusion of Cu atoms. To substantiate our claim, we carried out XRD analysis on a blanket Cu substrate before and after Ar annealing, and the resulting diffraction patterns exhibited a characteristic diffraction peak at 74° (220) for fcc Cu. Since the diffraction peaks of CuO and Cu_2O were obviously absent, we concluded that the Ar annealing process was conducted properly without undesirable oxygen interference. Hence, the presence of crystalline Cu_2O in our sample was attributed to the crystallization of amorphous Cu_2O which was formed when the Cu was immersed in the electroless bath. Because the pH value for the Ru electroless bath was between 11 and 12, according to the Pourbaix diagram, the thermodynamically stable state for the Cu was Cu_2O or CuO. Indeed, the Cu substrate immersed in an alkaline solution ($NaNO_{2(aq)} + NaOH_{(aq)} + NaClO_{(aq)}$, $p\mathrm{H} = 12.2$) for 120 min at 40°C revealed a diffraction pattern associated with amorphous CuO. After Ar annealing, both Cu and Cu_2O diffraction peaks became apparent. Therefore, we surmised that the formation of Cu_2O was caused by the corrosion reaction of Cu when the activated Si substrate was immersed in the alkaline plating bath. This Cu_2O was likely formed in the amorphous state initially but transformed to the crystalline structure after Ar annealing.

Figure 7 displays the XPS profiles of Ru 3d and Ru 3p for the as-deposited films along with curve fitting results of Ru $3p_{3/2}$. In general, the position of Ru 3d and Ru 3p lines are sensitive to the oxidative states of the Ru in the as-deposited film. In addition, their relative amount can be obtained via deliberate curve fitting of the

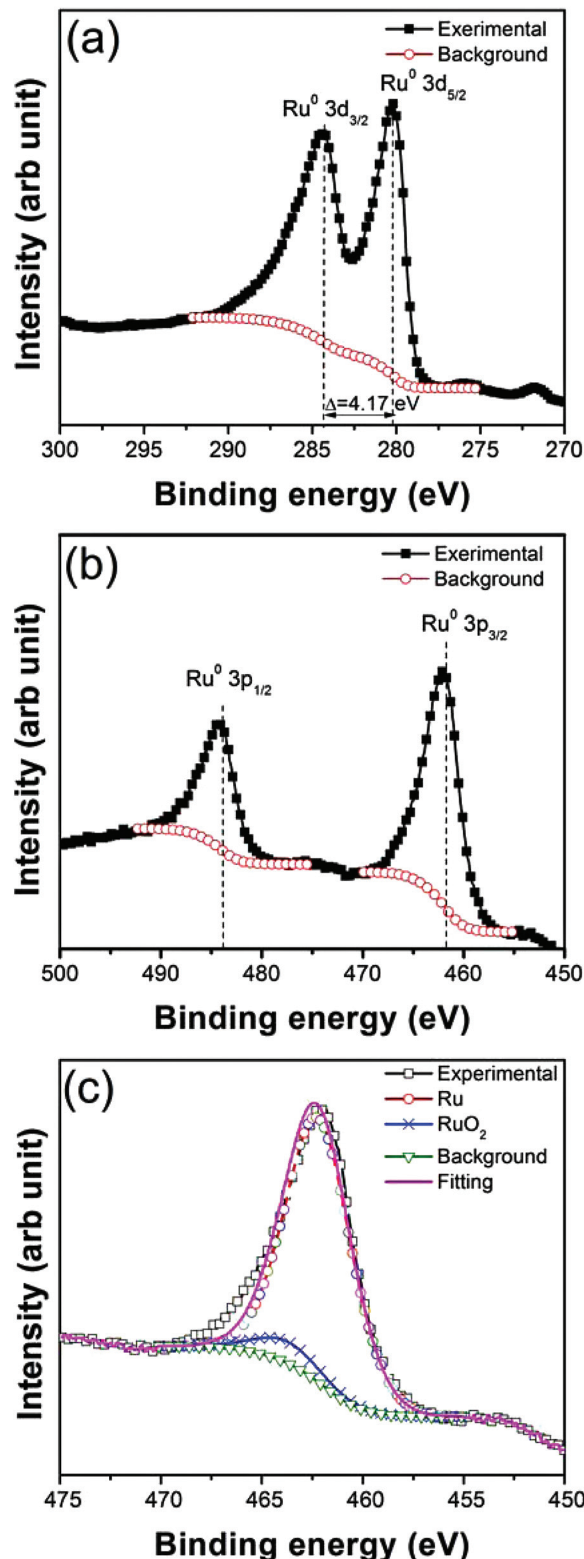

Figure 7. (Color online) XPS signals for the as-deposited film in (a) Ru 3d and (b) Ru 3p. Shown in (c) is the curve fitting result of Ru $3p_{3/2}$.

XPS profiles using binding energy of known Ru constituents. To achieve this objective, the Pt was presputtered on the as-deposited sample prior to the XPS analysis. In this way, we were able to use the Pt binding energy as a calibration. During the XPS measurements, the sample was cleaned by Ar bombardments and the recorded binding energy of Pt 4f was 71.3 and 74.6 eV, respectively.

Downloaded on 2014-04-24 to IP 140.113.38.11 address. Redistribution subject to ECS terms of use (see ecsdl.org/site/terms_use) unless CC License in place (see abstract).

Table I. Binding energy for Pt and Ru from XPS results and reference.

Element	Signal	Binding energy[a](eV)	Reference binding energy[b](eV)
Pt	$4f_{7/2}$	71.3	71.2
	$4f_{5/2}$	74.6	74.53
Ru	$3d_{5/2}$	280.2	280.1
	$3d_{3/2}$	284.4	284.27
Ru	$3p_{3/2}$	461.9	462
	$3p_{1/2}$	484.23	484

[a]From XPS results.
[b]From Ref. 34.

These values were reasonably close to 71.2 and 74.53 eV reported from earlier work.[33] As shown in Fig. 7a, the Ru $3d_{5/2}$ and Ru $3d_{3/2}$ signals were observed with binding energy of 280.2 and 284.4 eV. In addition, Fig. 7b exhibits the Ru $3p_{3/2}$ and Ru $3p_{1/2}$ signals with binding energy of 461.9 and 484.23 eV. Table I lists these values and the expected values of metallic Ru from literature.[34] Apparently, the XPS profiles for the as-deposited film indicated that a large proportion of the Ru existed in the metallic state. Figure 7c provides the curve fitting of Ru $3p_{3/2}$ using binding energy of 462.2 and 463.8 eV for Ru and RuO_2.[2] According to the curve fitting, the composition for the as-deposited film was 92.49 atom % Ru and 7.51 atom % RuO_2. XPS analysis on the Ru film after Ar annealing was not conducted because the XRD results had confirmed the presence of Ru phase after the Ar annealing step.

So far, we have established the presence of RuO_4, RuO_4^-, and RuO_4^{2-} in the plating bath and the deposit contained mostly metallic Ru with residual RuO_2 nearby. As both NaClO (oxidizer) and $NaNO_2$ (reducing agent) are present simultaneously in the plating bath, the sequence of possible chemical reactions that leads to the Ru deposition on the activated Si substrate is proposed below

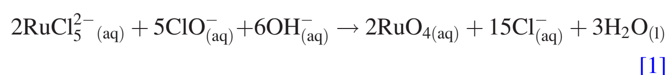

$$2RuCl_5^{2-}{}_{(aq)} + 5ClO^-_{(aq)} + 6OH^-_{(aq)} \rightarrow 2RuO_{4(aq)} + 15Cl^-_{(aq)} + 3H_2O_{(l)} \quad [1]$$

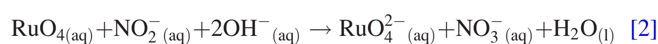

$$RuO_{4(aq)} + NO_2^-{}_{(aq)} + 2OH^-{}_{(aq)} \rightarrow RuO_4^{2-}{}_{(aq)} + NO_3^-{}_{(aq)} + H_2O_{(l)} \quad [2]$$

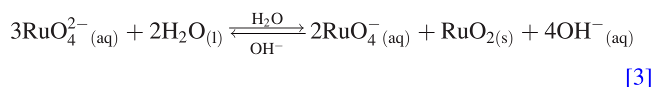

$$3RuO_4^{2-}{}_{(aq)} + 2H_2O_{(l)} \underset{OH^-}{\overset{H_2O}{\rightleftharpoons}} 2RuO_4^-{}_{(aq)} + RuO_{2(s)} + 4OH^-{}_{(aq)} \quad [3]$$

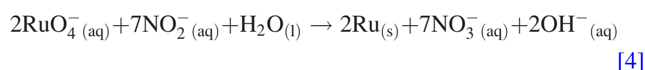

$$2RuO_4^-{}_{(aq)} + 7NO_2^-{}_{(aq)} + H_2O_{(l)} \rightarrow 2Ru_{(s)} + 7NO_3^-{}_{(aq)} + 2OH^-{}_{(aq)} \quad [4]$$

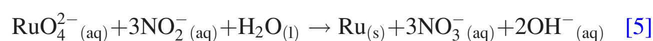

$$RuO_4^{2-}{}_{(aq)} + 3NO_2^-{}_{(aq)} + H_2O_{(l)} \rightarrow Ru_{(s)} + 3NO_3^-{}_{(aq)} + 2OH^-{}_{(aq)} \quad [5]$$

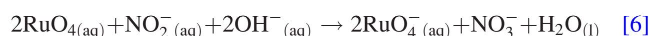

$$2RuO_{4(aq)} + NO_2^-{}_{(aq)} + 2OH^-{}_{(aq)} \rightarrow 2RuO_4^-{}_{(aq)} + NO_3^- + H_2O_{(l)} \quad [6]$$

To recapitulate the variation of the oxidized state for the Ru precursor in the electroless bath, a schematic for the complete reaction steps is illustrated in Fig. 8. As shown, the principal reaction route (Eqs. 1–5) is responsible for the deposition of metallic Ru and RuO_2. In Eq. 1, with NaOH in the solution, the NaClO is able to oxidize the $RuCl_5^{2-}$ forming a yellow RuO_4 colloidal suspension.[35,36] Since the RuO_4 is unstable chemically, it rapidly reacts with the $NaNO_2$ to convert to the RuO_4^{2-}, which appears in orange (Eq. 2). Afterward, two distinct routes are possible for the RuO_4^{2-}. First, a disproportionation reaction is likely to occur for the RuO_4^{2-}, which results in the formation of RuO_2 and RuO_4^- (Eq. 3).[37] Subsequently, the RuO_4^- quickly reacts with the $NaNO_2$ to produce the metallic Ru (Eq. 4). Alternatively, the RuO_4^{2-} adopts a straightforward reduction process in reacting with the $NaNO_2$ to produce the metallic Ru (Eq. 5). These reaction steps (Eqs. 1–5) are able to explain most of our experimental results except the transient presence of RuO_4^- during bath preparation shown in Fig. 2. Therefore, we surmise a secondary reaction path is likely to proceed via Eqs. 1, 4, and 6. In this route, the RuO_4 is reduced to the RuO_4^- initially which is reduced further to the metallic Ru.

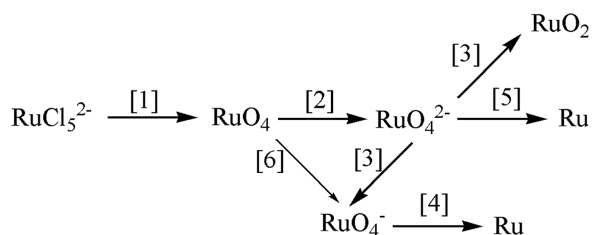

Figure 8. A schematic of the reaction path for the Ru precursor in electroless deposition.

It is noted that the electroless deposition of Ru thin film reported in this work is demonstrated on a Cu surface but the formula can in principle be applicable to other substrates including Si and ITO glass. However, in our experiences, additional surface pretreatments are necessary for Si and ITO glass to obtain a desirable Ru thin film and these results will be furnished and reported in the near future.

Conclusions

We developed an electroless Ru plating bath that enabled the deposition of Ru film on an activated Si substrate. Chemicals in the plating bath included Ru precursor ($K_2RuCl_5 \cdot xH_2O$), oxidizer (NaClO), stabilizer (NaOH), and reducing agent ($NaNO_2$). They were added simultaneously during bath preparation at 25°C to render a homogeneous solution for Ru deposition. Spectra from UV-Vis and XAS indicated that the $RuCl_5^{2-}$ was oxidized initially becoming RuO_4, followed by a slight reduction to RuO_4^{2-}. At this stage, the plating bath was ready for further reduction to the metallic form via a heterogeneous nucleation and growth. SEM images on the deposit revealed an integral film with scattered protrusions and cavities. Diffraction patterns from XRD indicated an amorphous nature for the as-deposited film, which was transformed to a crystalline phase after Ar annealing at 400°C for 2 h. Signals from XPS determined the film composition to be 92.49 atom % Ru and 7.51 atom % RuO_2.

Acknowledgment

Financial support from the National Science Council of Taiwan (98-2221-E-009-040-MY2) is noted. Discussion and assistance from Dr. J. F. Lee of National Synchrotron Radiation Research Center of Taiwan over XAS measurements and data analysis are greatly appreciated.

References

1. C. R. K. Rao and D. C. Trivedi, *Coord. Chem. Rev.*, **249**, 613 (2005).
2. K. H. Chang and C. C. Hu, *J. Electrochem. Soc.*, **151**, A958 (2004).
3. Y. S. Kim, H. I. Kim, M. A. Dar, H. K. Seo, G. S. Kim, S. G. Ansari, J. J. Senkevich, and H. S. Shin, *Electrochem. Solid-State Lett.*, **9**, C19 (2006).
4. K. Kawano, A. Nagai, H. Kosuge, T. Shibutami, N. Oshima, and H. Funakubo, *Electrochem. Solid-State Lett.*, **9**, C107 (2006).
5. E. M. Lysczek and S. E. Mohney, *J. Electrochem. Soc.*, **155**, H699 (2008).
6. S. Ogawa, N. Tarumi, M. Abe, M. Shiohara, H. Imamura, S. Kondo, and IEEE, in *IEEE International Intercconnect Technology Conference*, p. 102, Burlingame, CA (2008).
7. C. Xu, W. Li, and M. T. Cameron, U.S. Pat. Appl. Publ., Advanced Technology Materials Inc., US (2010). Pub. No.: US 2010/0209598 A1
8. D. Josell, D. Wheeler, C. Witt, and T. P. Moffat, *Electrochem. Solid-State Lett.*, **6**, C143 (2003).
9. Z. Yuan, R. J. Puddephatt, and M. Sayer, *Chem. Mater.*, **5**, 908 (1993).
10. C. Thambidurai, Y. G. Kim, and J. L. Stickney, *Electrochim. Acta*, **53**, 6157 (2008).
11. Y. Okinaka and C. Wolowodiuk, in *Electroless Plating: Fundamentals and Applications*, G. O. Mallory and J. B. Hajdu, Editors, p. 421, American Electroplaters and Surface Finishers Society, Orlando, Florida (1990).
12. K. Okuno, *Plat. Surf. Finish.*, **77**, 48 (1990).
13. Y. S. Chang and M. L. Chou, *J. Appl. Phys.*, **69**, 7848 (1991).
14. M. Rarnani, B. S. Haran, R. E. White, and B. N. Popov, *J. Electrochem. Soc.*, **148**, A374 (2001).

Downloaded on 2014-04-24 to IP 140.113.38.11 address. Redistribution subject to ECS terms of use (see ecsdl.org/site/terms_use) unless CC License in place (see abstract).

15. T. Jones, in *Electroplating of the Lesser-known Precious Metals: Rhodium, Ruthenium, Iridium, Rhenium, Osmium*, p. 87, Finishing Publications Limited, Herts (2003).
16. A. Zieliene, l. Vaskelis, and E. Norkus, U.S. Pat., Lam Research Corporation, US Pat. No. US 7,682,431 B1 (2010).
17. M. Hasegawa, N. Yamachika, Y. Shacham-Diamand, Y. Okinaka, and T. Osaka, *Appl. Phys. Lett.*, **90**, 101916 (2007).
18. K. I. Popov, S. S. Djokic, and B. N. Grgur, in *Fundamental Aspects of Electrometallurgy*, p. 250, Kluwer Academic/Plenum Publishers, New York (2002).
19. A. M. Fundo and L. M. Abrantes, *J. Electroanal. Chem.*, **600**, 63 (2007).
20. P. T. Liu, Y. T. Chou, C. Y. Su, and H. M. Chen, *Surf. Coat. Technol.*, **205**, 1497 (2010).
21. S. S. Djokić, *J. Electrochem. Soc.*, **151**, C359 (2004).
22. Y. Okinaka and K. Masaru, in *Modern Electroplating*, 4th ed., M. Schlesinger and M. Paunovic, Editors, p. 705, John Wiley & Sons., New York (2000).
23. S. S. Djokić, *Plat. Surf. Finish.*, **86**, 104 (1999).
24. C. M. Chen, C. H. Chen, S. J. Cherng, and T. C. Wei, *Mater. Chem. Phys.*, **124**, 173 (2010).
25. T. Jones, in *Electroplating of the Lesser-known Precious Metals: Rhodium, Ruthenium, Iridium, Rhenium, Osmium*, p. 3, Finishing Publications Limited, Herts (2003).
26. S. L. Cheng and H. C. Peng, *J. Electrochem. Soc.*, **157**, D81 (2010).
27. J. H. Han, S. W. Lee, S. K. Kim, S. Han, C. S. Hwang, C. Dussarrat, and J. Gatineau, *Chem. Mater.*, **22**, 5700 (2010).
28. E. A. Seddon, in *The Chemistry of Ruthenium*, p. 51, Elsevier, Amsterdam (1984).
29. M. Pagliaro, S. Campestrini, and R. Ciriminna, *Chem. Soc. Rev.*, **34**, 837 (2005).
30. Y.-C. Hsieh, L.-C. Chang, P.-W. Wu, Y.-M. Chang, and J.-F. Lee, *Appl. Catal., B*, **103**, 116 (2011).
31. E. A. Seddon, in *The Chemistry of Ruthenium*, p. 58, Elsevier, Amsterdam (1984).
32. E. A. Seddon, in *The Chemistry of Ruthenium*, p. 57, Elsevier, Amsterdam (1984).
33. J. F. Moulder, W. F. Stickle, P. E. Sobol, and K. D. Bomben, in *Handbook of X Ray Photoelectron Spectroscopy: A Reference Book of Standard Spectra for Identification and Interpretation of XPS Data*, J. Chastain and J. R. C. King, Editors, p. 181, Physical Electronics Eden Prairie, Minnesota (1995).
34. J. F. Moulder, W. F. Stickle, P. E. Sobol, and K. D. Bomben, in *Handbook of X Ray Photoelectron Spectroscopy: A Reference Book of Standard Spectra for Identification and Interpretation of XPS Data*, J. Chastain and J. R. C. King, Editors, p. 115, Physical Electronics Eden Prairie, Minnesota (1995).
35. S. Wolfe, S. K. Hasan, and J. R. Campbell, *J. Chem. Soc. D*, 1420 (1970).
36. E. A. Seddon, in *The Chemistry of Ruthenium*, p. 49, Elsevier, Amsterdam (1984).
37. E. A. Seddon, in *The Chemistry of Ruthenium*, p. 73, Elsevier, Amsterdam (1984).

Downloaded on 2014-04-24 to IP 140.113.38.11 address. Redistribution subject to ECS terms of use (see ecsdl.org/site/terms_use) unless CC License in place (see abstract).